Ceramics International 49 (2023) 19569–19577

Contents lists available at ScienceDirect

Ceramics International

journal homepage: www.elsevier.com/locate/ceramint

Review article

Synthesis and properties of Zn and Zn–Mg-doped tricalcium phosphates obtained by Spark Plasma Sintering

Maria Antonia Sainz *, Sara Serena, Angel Caballero

Institute of Ceramics and Glass (ICV-CSIC), Madrid, Spain

ARTICLE INFO

Handling Editor: Dr P. Vincenzini

Keywords:
TCP
Zn-TCP
Zn–Mg-TCP
Spark plasma sintering
Mechanical characterization
Biological behavior

ABSTRACT

β-tricalcium phosphate ($Ca_3(PO_4)_2$ or TCP) are essential biomaterials because of the chemical composition, high biocompatibility and osseointegration. However, their limited mechanical properties restrict their use to areas where high mechanical performances are not required. Spark Plasma Sintering (SPS) was selected out of the unconventional sintering methods in order to obtain high-density doped-TCP bioceramic materials. The main advantages of SPS are a high heating rate, low sintering temperatures and short residence times, producing bioceramics with full density and fine-grain microstructure. The main purpose was to design, obtain by SPS and characterize undoped β-TCP, 1ZnO-doped β-TCP and 1ZnO-1MgO codoped β-TCP (wt. %) bioceramics. All the obtained samples were visually semitransparent and mainly β-TCP was detected by X-ray analysis. Densification behavior was determined by Archimedes' method and microstructural features of the sintered specimens were analyzed by Field Emission Scanning Electron Microscopy (FE-SEM-EDX). The undoped and doped β-TCP bioceramics were mechanically characterized, specifically the modulus of elasticity and Vickers microhardness. The results are compared with equivalent samples obtained by conventional solid-state sintering (CS) reaction. A first study of biological behavior was carried out, specifically direct cell adhesion of MG-63 human osteoblast-like cells on the polished surfaces of β-TCP, 1ZnO-β-TCP and 1ZnO–1MgO-β-TCP dense samples were determined. The present study concludes that the SPS process together with the doping effect enhanced sinterability, mechanical and biological properties of Zn-TCP and Zn–Mg-TCP based materials.

1. Introduction

Calcium phosphate biomaterials have been developed as a synthetic alternative for the bone fixation and replacement of damaged or lost bones caused by tumor resection, traumas or malformations. The main objective is to design a material capable of supporting the initial loads, transferring them progressively to the new bone during its degradation. Calcium phosphate ceramics although could be considered the "ideal" biomaterials, due to their chemical composition, high biocompatibility and osseointegration [1], present the inconvenience of their limited mechanical properties [2,3]. Its mechanical strength is severely affected by the difficulty to sinter highly dense β-TCP polymorph materials due to the low temperature β→α-TCP phase transition (1125 °C [4,5]) which involves a large expansion (7%) causing microcracks and its high dissolution in the human biological environment, compared to new bone development during the progressive degradation of old bone [6,7]. These facts restrict their use to areas where high mechanical performances are not required, such as coatings on metal prostheses, composite materials and calcium phosphate cements. In order to improve the materials sinterability, few authors report on electrical assisted sintering methods to obtain dense TCP at lower temperatures. Frasnelli et al. [8] obtained TCP with high density by flash sintering, an electrical field assisted consolidation, and Zhang et al. [9] and Kawagoe et al. [10] who prepared dense β-TCP ceramics by Spark Plasma Sintering (SPS), a pressure-assisted pulsed-current process in which the powder samples are sintered under a uniaxial pressure. Recently, other authors report the sintering of ceramics at low temperature by cold sintering process [11], obtaining samples for calcium phosphate materials between 75 and 85% of theoretical density [12].

The interest in Zn^{2+} and Mg^{2+} as TCP dopants is that they significantly increase the range of thermal β→α-TCP phase transition, improving the stability of the β-TCP phase [13–15] and also the bone metabolism. This point is of particular interest because both polymorphs of TCP are biodegradable and release Zn, Mg, Ca and P to the human biological environment. Zinc is a very important trace element in the human body that is useful to promote biological functions [16–18].

* Corresponding author.
E-mail address: masainz@icv.csic.es (M.A. Sainz).

https://doi.org/10.1016/j.ceramint.2023.03.104
Received 12 January 2023; Received in revised form 7 March 2023; Accepted 10 March 2023
Available online 11 March 2023

Thus, due to its excellent osteogenic properties zinc helps in bone formation and calcification and DNA formation [19]. Recently, the antibacterial properties of Zn have also been put in evidence, which opens up a new scope of fabricating implants containing zinc with improved antibacterial properties [19–21]. Moreover, magnesium plays an important role in bone remodeling, proliferation and stimulation of osteoblastic cell growth and DNA stabilization [22–25].

In the present work, we used the unconventional sintering method Spark Plasma Sintering (SPS). This method consist in applying a pulsed electric current and a uniaxial mechanical pressure during the thermal cycle for obtaining high-density ceramic materials. The main advantages of the SPS compared to the conventional sintering methods used so far, are a faster heating rate and lower-temperature sintering which allows controlling the microstructural development, limiting the crystalline size and driving to high-density materials with better mechanical properties. In this way, Zhang et al. [9] and Kawagoe et al. [10] prepared macroporous calcium phosphate scaffolds from nanocrystalline powders and transparent β-TCP ceramics by SPS respectively with the aim of optimizing microstructure to improve TCP mechanical properties. However, the effect of SPS on the properties (and specifically mechanical properties) of Zn-doped TCP and Zn, Mg codoped-TCP have not been reported. The aim of this research is to discuss their properties and improve the scope of the biomedical application of doped TCP biomaterials.

For this purpose, SPS sintering tests were carried out on doped (1.0 ZnO wt. % and 1.0 ZnO-1.0 MgO wt. %), and undoped samples of TCP. These compositions were chosen taking into account previous results, in which the solid solution extension region of Zn^{2+} in the TCP structure system was delimitated [26]. A sintering temperature of 1100 °C/5min was selected and 50 MPa of load was applied automatically during the process; all the tests were carried out in a vacuum atmosphere of 4 MPa. A complete physical, chemical, microstructural and mechanical characterization of SPS biomaterials obtained was carried out. The results were compared with materials obtained by conventional pressureless solid-state sintering in air at 1100 °C for 12 h, at a heating/cooling rate 3 °C/min. Finally, the direct interaction of undoped β-TCP, 1ZnO-TCP and 1ZnO–1MgO-TCP dense biomaterials with MG-63 osteoblasts cells was analyzed.

2. Material and methods

2.1. Materials

The commercial raw materials used in this study were ammonium dihydrogen phosphate ($NH_4H_2PO_4$, purity ≥99.0%, Fluka, with a specific surface = 0.1 m^2/g and d_{50} = 427.5 μm), calcium carbonate ($CaCO_3$, purity ≥99.0%, Panreac, with a specific surface of 1.1 m^2/g and d_{50} = 16.7 μm), zinc oxide (ZnO, purity ≥99.9%, Agalsa, with a specific surface of 6.5 m^2/g and d_{50} = 1.0 μm) and magnesium oxide (MgO, purity ≥97.0%, Merck, with a specific surface of 26.0 m^2/g and d_{50} = 13.0 μm). As the powder precursors presented a wide dispersion of particle sizes specially $NH_4H_2PO_4$, this compound was previously milled in an attrition-mill in isopropyl media using zirconia balls for 4 h. The average particle size obtained was d_{50} = 28.4 μm, closer to the other reagents used.

The selected compositions were undoped β-TCP (named TCP), zinc oxide doped-TCP (named 1Z-TCP) and zinc oxide-magnesium oxide codoped TCP (named 1Z-1M-TCP). The compositions selected in oxides are shown in Table 1.

The compositions studied were prepared by mixing starting powders in an attrition-mill using Y-ZrO_2 balls in isopropyl media for 4 h. After the milling step, the powders were oven dried at 60 °C for 24 h, crushed and sieved through a 63 μm mesh. Subsequently, the compositions were synthesized by conventional solid-state sintering at 900 °C for 4 h according to Carbajal et al. [13].

The synthesis of undoped, doped and codoped compositions for obtaining β-TCP materials was completed according to the following reactions.

$$3\ CaCO_3 + 2\ NH_4H_2PO_4 \rightarrow Ca_3(PO_4)_2 + \uparrow 3H_2O + \uparrow 2\ NH_3 + \uparrow 3CO_2 \quad \text{(equation 1)}$$

$$X\ ZnO + (3\text{-}X)\ CaCO_3 + 2\ NH_4H_2PO_4 \rightarrow [Zn_XCa_{(3\text{-}X)}](PO_4)_2 + \uparrow 3H_2O + \uparrow 2\ NH_3 + \uparrow (3\text{-}X)\ CO_2 \quad \text{(equation 2)}$$

$$X\ ZnO + Y\ MgO + (3\text{-}X\text{-}Y)\ CaCO_3 + 2\ NH_4H_2PO_4 \rightarrow [Zn_XMg_YCa_{(3\text{-}X\text{-}Y)}](PO_4)_2 + \uparrow 3H_2O + \uparrow 2\ NH_3 + \uparrow (3\text{-}X\text{-}Y)\ CO_2 \quad \text{(equation 3)}$$

After synthesis, compositions were milled in an attrition-mill using Y–ZrO_2 balls in isopropyl media for 2 h. After the milling step, the powders were oven dried at 60 °C for 24 h, crushed and sieved through a 63 μm mesh. The specific surface and average grain size were 7.0 m^2/g and d_{50} = 1.07 μm respectively.

2.2. Thermal treatment

The SPS sintering tests of β-TCP powders previously obtained were performed in the SPS furnace (SPS-510CE, SPS Syntex Inc, Japan). Cylindrical pellets with a diameter of 20 mm and 4 mm thickness were obtained by uniaxial pressing of synthesized powders (4 g.) at 2 MPa. Before SPS treatment, samples were fully covered with a Pt jacket in order to avoid carbon contamination from the graphite furnace and were placed in a graphite crucible and sintered by pulse-current pressure firing. A sintering temperature of 1100 °C for 5 min was selected (temperature lower than that of β→α-TCP total transformation) at a heating rate of 50 °C/min between 50 and 800 °C and 25 °C/min between 800 and 1100 °C in order not to exceed said temperature during test. Temperature was controlled with a pyrometer focalized in a hole drilled on the surface of the graphite die. A uniaxial load of 50 MPa was applied during the heating holding cycle and subsequently was reduced to 20 MPa on cooling. All tests were carried out in a vacuum atmosphere of 4 MPa. At least 4 runs were performed for each composition.

Sintering parameters, voltage, current intensity, temperature, vacuum pressure, uniaxial pressure and displacement with respect to the Z-axis (dz) were recorded continuously during tests.

For comparative purposes, conventional sintering CS tests were performed in samples with a diameter of 10 mm and 4 mm thickness prepared from cylindrical pellets obtained by isostatic pressing at 200 MPa of synthesized powders. Samples were placed in a Pt crucible to avoid contamination and were pressureless sintering in air at 1100 °C for 12 h, at a heating/cooling rate of 3 °C/min.

2.3. Characterization of powders and samples

High temperature dilatometry was performed in a differential

Table 1
Compositions selected.

Named compositions	% Weight				% Mol			
	ZnO	CaO	P_2O_5	MgO	ZnO	CaO	P_2O_5	MgO
TCP	–	54.235	45.765	–	–	75.00	25.00	–
1Z-TCP	1.000	53.377	45.623	–	0.956	74.044	25.000	–
1Z-1M-TCP	1.000	52.200	45.800	1.000	0.952	72.125	25.000	1.923

dilatometer Netzsch 407/E, from plane-parallel cylinders of 10 mm diameter and 8 mm high obtained from isostatic pressing at 200 MPa of synthetized initial powders. Cylinders were treated at a heating rate of 3 °C/min up to 1400 °C. During data treatment, the expansion/contraction of the support, determined in a previous calibration process, was subtracted.

TCP, 1Z-TCP and 1Z-1M-TCP SPS-materials were characterized in terms of compositional, structural, mechanical and biological properties. Linear shrinkage (dz) curves versus temperature from SPS process were analyzed. Densities of the sintered samples were determined using the Archimedes method in water and 3.08 g/cm^3 was the density value taken as reference to undoped β-TCP. Identification of crystalline phases was performed from by X-ray diffraction (XRD) measurements in Bragg-Brentano geometry using a Bruker D8 Advance diffractometer (Bruker, Germany) with lynx eye and monochromatic Cu $K\alpha_1$ (λ = 1.5406 Å) radiation. Phase identification was done using PDF-2 release 2000 crystallographic database using ICDD's integrated data. The Ca/P, Ca + Zn/P and Ca + Zn + Mg/P molar ratio was determined by inductively coupled plasma-optical emission spectroscopy (ICP-OES IRIS ADVANTAGE (Thermo Jarrel Ash, USA)) for all thermal treated compositions studied. The surface rough of the sintered polished disks was determined using a PerthometerM1 (Mahr GMbH, Germany). The obtained roughness parameters were Ra = average roughness and Rz = mean roughness depth (ISO 4287).

Microstructure, porosity and grain size of the crystalline phases present were evaluated on polished and chemically etched with acetic acid (10%) samples using a Field Emission Scanning Electron Microscopy FE-SEM (Hitachi S-4700, Tokio, Japan), equipped with Energy Dispersive Spectroscopy (EDS). Mechanical properties were characterized on polished samples by Vickers microhardness using a Zwick/Roell, Zhu 2.5 equipment (Zwick GmbH & Co. KG, Germany). A load of 98 N for 15s was applied. A total of 15 indents per samples were measured.

The evaluation of "in vitro" direct cell-surface material adhesion, distribution and morphology was evaluated using a confocal laser-scanning microscope (CLSM, TCS SP2; Leica Microsystems, Germany). The images obtained were acquired and processed using the Leica confocal software (version 2.0). MG-63 human osteoblasts-like cells were cultured in flasks containing 12 ml of culture medium with 1% of penicillin + glutamine. Cells were maintained at 37 °C in a humidified atmosphere of 5% CO_2 in air, the medium was changed every 2–3 days until confluence following the procedure described by Carbajal et al. [14]. After 48 h, the samples were evaluated for cell adhesion, distribution and morphology using a confocal laser scanning microscope (CLSM Leica). For this reason, the samples were removed from the well plates, covered with PBS and stored in the dark. CLSM images were acquired and processed using Leica Software. Each experiment was repeated with five samples.

3. Results and discussion

3.1. Sintering process

Advanced (SPS) sintering process was monitored by registering the displacement with respect to the Z-axis in the contraction curve for SPS samples, with a heating rate of 50 °C/min between 50 and 800 °C and 25 °C/min between 800 and 1100 °C. For conventional sintering (CS) samples were monitored by high temperature dilatometry (HTDIL) curves, recorded at a heating rate of 3 °C/min. The contraction data, recorded in the SPS curves, were corrected to subtract the signal due to graphite, which was obtained in a previous calibration process in the same conditions. In the case of HTDIL, expansion of the support and the probe determined in a previous calibration process, were also subtracted.

From Fig. 1 different points should be considered. First, shrinkage

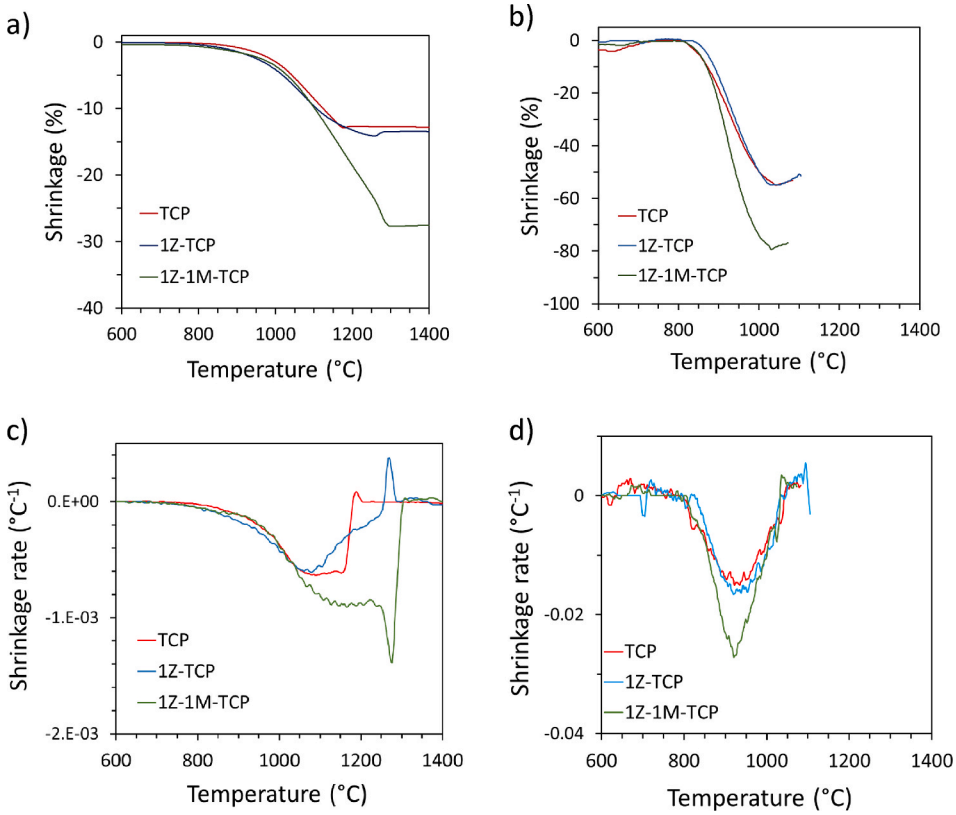

Fig. 1. Linear shrinkage and lineal shrinkage rate (dz/dT) curves as a function of temperature of undoped and doped TCP samples are shown. a and c) CS samples up to 1400 °C, with a heating rate of 3 °C/min; b and d) SPS tests up to 1100 °C, with a heating rate of 50 °C/min between 50 and 800 °C and 25 °C/min between 800 and 1100 °C.

starts at 850 °C and 950 °C in the case of SPS and CS samples respectively and the slopes of the curves in SPS tests (Fig. 1b) fall faster than the equivalent curves obtained in CS tests (Fig. 1a). All the shrinkage curves have two steps, shrinkage due to particle rearrangement and densification and further sintering. A slight expansion effect was observed in undoped TCP and 1Z-TCP CS samples.

Second, it is noteworthy that the behavior of undoped-TCP and 1Z-TCP was very similar in terms of shrinkage and showing only a slight temperature increase in the end of shrinkage. It is also relevant that 1Z-1M-TCP sample shows in both tests a significantly higher shrinkage and, especially in CS tests, the highest temperature, 1300 °C, at which shrinkage ends. In SPS tests, shrinkage ended between 1000 and 1025 °C, in all samples. Moreover, the temperatures of maximum shrinkage in CS test were 1182 °C, 1250° and 1300 °C for undoped-TCP, 1Z-TCP and 1Z-1M-TCP respectively (Fig. 1a), and between 1000 and 1025 °C, for all samples in the case of SPS test (Fig. 1b). As a consequence, SPS treatment always leads to maximum shrinkage at temperatures 150-300 °C lower than CS.

At working temperature in both CS and SPS test, permanent liquid phase is not a stable phase according to the information supplied by $Ca_3(PO_4)_2$–$Zn_3(PO_4)_2$, $Ca_3(PO_4)_2$–$Mg_3(PO_4)_2$ and $Ca_3(PO_4)_2$–$Zn_3(PO_4)_2$–$Mg_3(PO_4)_2$ phase equilibrium diagrams [26–28]. Therefore, it can be suggested that both sintering processes took place in solid state. Nevertheless, SPS process occurs through complex mechanisms involving evaporation from particle surface, formation of a plasma or a hot polarized gas, surface and volume diffusion and condensation in the gap left between particles [29]. These mechanisms should be the cause of the differences found during sintering between both thermal treatments.

The study of the shrinkage rate curves give us some insights to understand the differences in the behavior of the samples during heating. Fig. 1 shows the lineal shrinkage rate of CS (Fig. 1c) and SPS (Fig. 1d) samples versus temperature. The shrinkage rate curves of CS samples show specific points, which put in evidence the different and sequential processes that occur during densification step. On the contrary, in SPS tests, only one point of maximum shrinkage rate was observed in all samples, indicating that densification takes place in a single step.

Focusing on the case of CS samples (Fig. 1c), the maximum of shrinkage rate of undoped TCP sample occurs in the range of 1075°C-1170°. At higher temperature a sudden decrease in the shrinkage rate is detected and finally a weak peak is observed at 1195 °C which can be related to the slight expansion effect detected in the shrinkage curve of TCP (Fig. 1a) previous to the end of densification. In the sample 1Z-TCP a continuous increase of shrinkage rates up to 1075 °C is observed and from this temperature a progressive decrease of shrinkage rate is detected up to 1270 °C when a sharp peak is observed in good agreement with the expansion effect detected in Fig. 1a. Sample 1Z-1M-TCP shows a first step of maximum shrinkage rate between 1140° to 1240 °C, followed of a sharp increase of shrinkage rate up to 1270 °C from which a sudden decreases of shrinkage rate takes place again associated to the end of densification.

In the case of SPS treatment (Fig. 1d), the shrinkage rate of all samples was greater than CS tests and the maximum shrinkage rate took place at the same temperature (900 °C), which is clearly lower to that of the β to α-TCP transformation and as a consequence no expansion effect was detected in these samples. In this SPS treatment, it can be concluded that densification process took place in one-step, being remarkable that the temperature of beginning and end of the densification process were similar in all studied samples.

The behavior observed in CS samples can be explained in terms of the β to α-TCP transformation on heating. The maximum shrinkage rate, in all samples, takes place during densification process at temperatures lower than β→ α-TCP transformation [4,5] and the expansion effect observed in undoped TCP and 1Z-TCP sample at higher temperature was the consequence of the volume increased produced by β to α-TCP transformation. On the other hand, no expansion effect at high temperature was observed in 1Z-1M-TCP composition indicating that β→ α-TCP transformation did not occur in this sample in the range of temperature studied. The behavior of codoped sample is justified by the strong stabilizing effect of Mg^{2+} + Zn^{2+} ions on β-TCP phase, which delays the start of the β to α polymorphic transformation of TCP, in good agreement with the information supplied by the corresponding phase equilibria diagrams [26–28]. The stabilizing effect of both cations is associated to the substitution of Ca^{2+} in the structure of β-TCP, in Ca(5) position [30,31]. Furthermore, these diagrams also show that Mg^{2+} compared to Zn^{2+} stabilizes β-TCP in a greater range of temperatures and compositions. Therefore, the presence of Zn^{2+}, in sample 1Z-TCP, delays the end of densification and the beginning of the β→α transformation by approximately 75 °C compared to undoped TCP sample. On the other hand, the end of densification is delayed more than 150 °C in the case of 1Z-1M-TCP composition.

These results revealed the differential effect produced by the solid solution of 1% ZnO +1% MgO respect to solid solution of 1% of ZnO which is attributed not only to a higher dopant content (2% vs 1%) but also to the greater stabilizing effect of magnesium compared to zinc as was previously mentioned.

3.2. Characterization of SPS samples

The XRD qualitative Rietveld analysis of the crystalline phases present in sintered SPS samples, allowed us to identify the characteristics diffractions of β-TCP (ICDD No. 70–2065) in all samples and a small amount of Hydroxyapatite (HAP) (ICDD No 86–0740) in undoped and 1Z-TCP samples (Fig. 2). Codoped sample consisted of β-TCP while undoped TCP and 1Z-TCP samples consisted of β-TCP and around 5% and <2% of HAP respectively. Likewise, the absence of diffractions associated with ZnO or MgO presence together with the slight displacement observed in the main diffraction of β-TCP, higher in the case of codoped samples, enlargement Fig. 2, confirmed the incorporation of Zn^{2+} and Mg^{2+} in solid solution, substituting to Ca^{2+} into the TCP crystal structure.

An inductively coupled plasma-optical emission spectroscopy (ICP-OES) analysis showed that (Mg + Zn + Ca)/P molar ratio of sintering samples was 1.52 ± 0.02 indicating that samples were slightly enriched in calcium oxide, which justifies the presence of the small amount of hydroxyapatite observed in XRD of undoped and 1Z-TCP SPS samples.

The evolution of lattice parameters of β-TCP phase of SPS samples was also established (Table 2). A decrease in lattice parameters with the increase in dopant content was observed.

This fact is a consequence of the lower ionic radius, for six

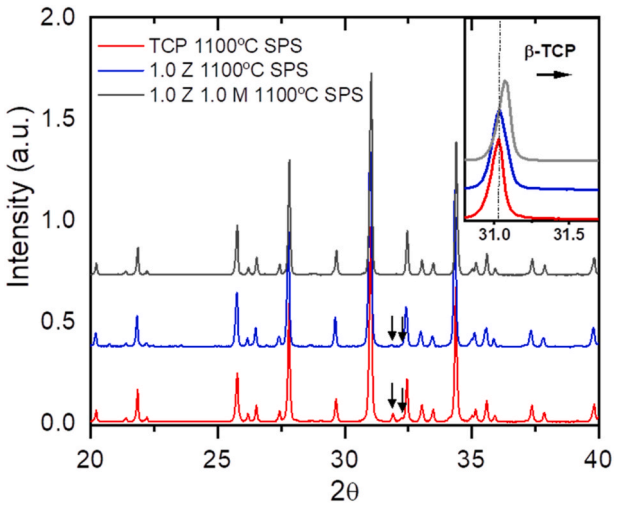

Fig. 2. XRD diffractions pattern of undoped and doped TCP SPS samples. (↓Hydroxyapatite).

Table 2
β-TCP lattice parameters of samples obtained by SPS.

SPS samples	a, b (Å)	c (Å)	Volume
TCP (1100 °C)	10.4333 ± 0.0004	37.406 ± 0.002	3526.2 ± 0.3
1Z-TCP(1100 °C)	10.4225 ± 0.0004	37.388 ± 0.002	3517.3 ± 0.3
1Z-1M-TCP (1100°C)	10.4134 ± 0.0003	37.375 ± 0.002	3509.9 ± 0.2

coordination, of Zn^{2+} (0.73 Å) and Mg^{2+} (0.72 Å), with respect to Ca^{2+} (1.00 Å) [32]. Either of these two metals with smaller ionic radius can easily be incorporated in Ca(5) position of the β-TCP structure as it was commented earlier. This tactical substitution of Ca^{2+} by Zn^{2+} and Mg^{2+} produces a decrease in lattice TCP parameters enhancing densification and sintering processes and as a consequence it is expected an improvement of thermal stability and properties of samples, specially the mechanical properties of SPS samples due to high densities and very limited grain growth generally obtained in SPS treatments.

Moreover, from the biological point of view, once the biomaterial is implanted, the controlled release of Zn^{2+} and Mg^{2+} will supply the physiological environment locally, combining the benefits of both dopants with desirable biological properties such as, stimulation of bone growth and its mineralization, osteogenic differentiation, bactericidal effect and improved the proliferation of osteoblasts [21–25,33,34].

Fig. 3 shows optical micrographs of samples obtained by SPS (1100 °C/5min). The samples have a white-translucent appearance, which makes it clear that there is no graphite contamination from SPS graphite furnace in them. Also, neither bending and nor cracking were observed. The apparent densities of samples varied between 3.035 and 3.075 g/cm^3 very close to the theoretical density (3.08 g/cm^3) and therefore extremely low porosity values less than 2% were obtained, as it is expected in SPS treatments. In contrast, maximum density values obtained in CS samples, between 88 and 95% of the theoretical density (Fig. 4) were significantly lower than that obtained in SPS samples (98–100% of theoretical density).

The microstructure of SPS polished samples is shown in Fig. 5, without and with chemical etch (acetic acid 10% vol). No porosity was observed in not etched samples (Fig. 5a, c and e) according with the high values of densities obtained in SPS treatment. In etched samples (Fig. 5b, d and f), a very limited crystalline growth was observed. Grain size ranging from 1 to 2 μm in undoped TCP sample to 0.5 μm in 1Z-1M-TCP and small amount of porosity (≤3%), mainly in grain boundary, was detected in undoped TCP (Fig. 5b) while almost null porosity (≤1%), was observed in 1Z-TCP and 1Z-1M-TCP compositions (Fig. 5d and f). Likewise, a very small amount of dispersed white crystals lodged in the β-TCP matrix and doped 1Z-TCP (Fig. 5b and d) was detected in all samples. The presence of this phase, identified by XRD as hydroxyapatite (HAP), was a consequence of a slight excess of Ca/P ratio in all synthesized starting powders.

For comparative purposes, CS chemically etched (acetic acid 10% vol.), polished samples (Fig. 6) were analyzed. As can be seen, both intergranular porosity and crystal size showed higher values. In the case of undoped TCP sample grain size and porosity values were 3–4 μm and ≈10% respectively. In the sample 1Z-TCP, grain size increased strongly up to 7–10 μm while porosity decreased slightly until ≈7%. Finally,

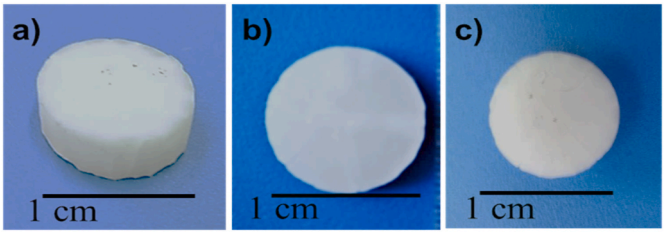

Fig. 3. Optical micrograph of SPS samples. a) undoped TCP, b) 1Z-TCP and c) 1Z-1M-TCP.

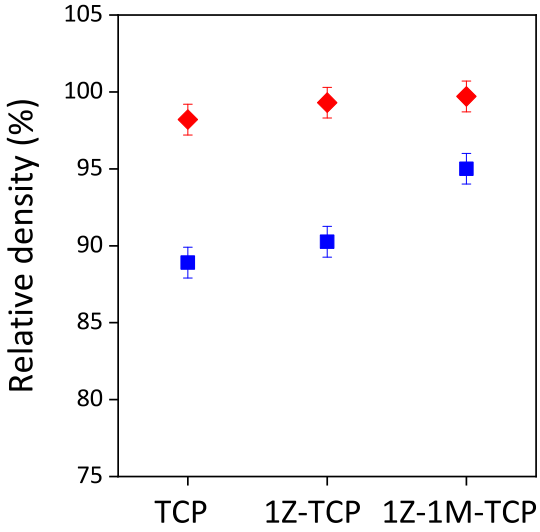

Fig. 4. Relative density of undoped and doped TCP samples obtained by SPS (◆) and conventional sintering (CS) (■) at 1100 °C.

sample 1Z-1M-TCP shows the same trend, more grain growth (10–20 μm) together with a lower porosity (≈5%).

Finally, note that SPS translucent samples showed an average grain size between 0.5 and 1.5 μm, being relevant that sample 1Z-1M-TCP showed smaller grain size than 1Z-TCP sample. Conventional sintering samples showed a grain size of almost an order of magnitude higher than those observed in SPS samples while porosity was always higher except for 1Z-1M-TCP sample. Both effects are a clear consequence of the different sintering methods used.

3.3. Mechanical characterization

The ceramic biomaterials obtained by both sintering methods were mechanically characterized, determining their modulus of elasticity (E) and their Vickers microhardness (Hv).

The elastic modulus and Vickers microhardness were determined according to the Oliver and Pharr method of 1992 [35], implemented in the micro-indentation equipment used.

The Vickers hardness value (Hv) in Pa was obtained from the indentation trace using the following equation [36]:

$$Hv = 0.47\frac{P}{r^2} \quad \text{(equation 4)}$$

Where P is the applied load in N and r is the radius of indentation print in mm.

The modulus of elasticity (E) was calculated by the equipment software from the load-penetration curves, considering the linear area of the discharge curve and its slope in the interval 60–95% of the discharge. The calculation of E was carried out using the following expressions [37]:

$$\frac{dP}{dH} = \frac{2}{\sqrt{\pi}}E^*\sqrt{A} \quad \text{(equation 5)}$$

Where P is the applied load, h is the penetration achieved and E* is the modulus of elasticity of the material, which is given by:

$$\frac{1}{E^*} = \frac{1-\nu_s^2}{E_s} + \frac{1-\nu_I^2}{E_I} \quad \text{(equation 6)}$$

Where ν is Poisson's ratio and the subscripts, S and I correspond to the substrate and the diamond indenter, respectively. A value of 0.26 of Poisson's ratio was used for these TCP materials, in agreement with the range (0.22–0.3) reported in the literature [38,39].

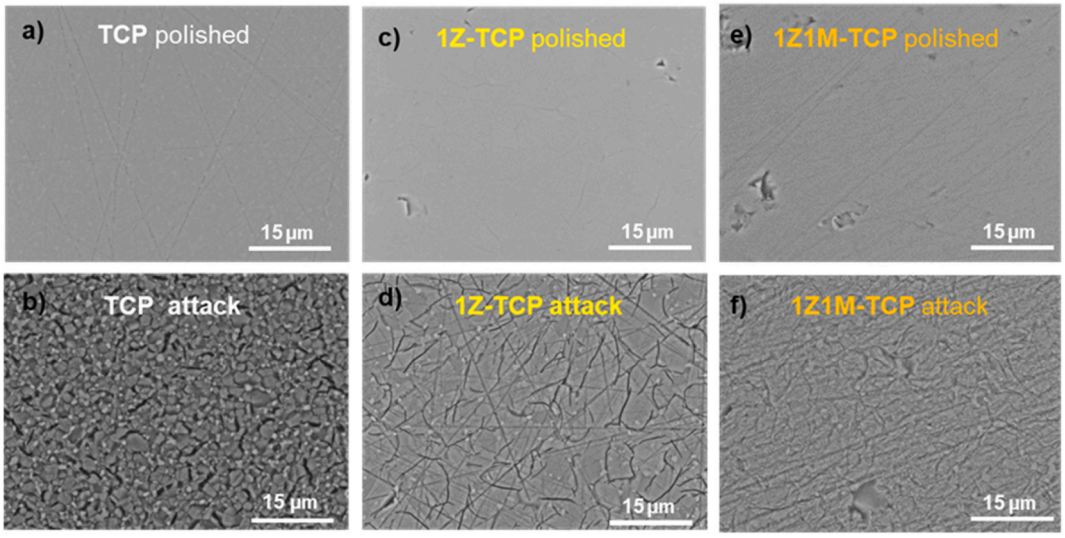

Fig. 5. FE-SEM micrographs of polished surface of SPS samples (1100 °C/5min.) with or without chemical attack: a) and b) correspond to undoped-TCP; c) and d) to 1Z-TCP; e) and f) to 1Z-1M-TCP.

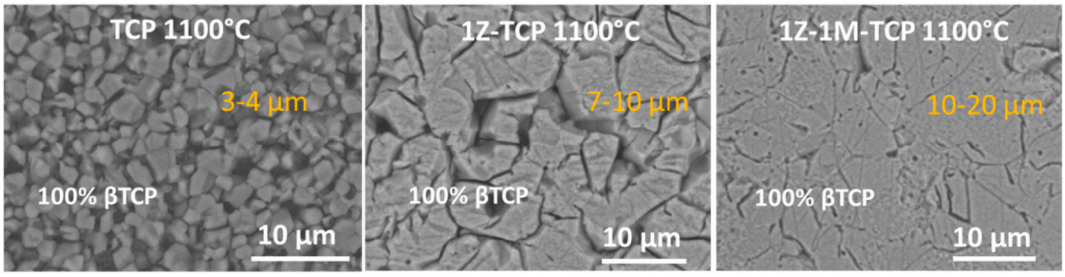

Fig. 6. FE-SEM micrographs of polished surface of CS samples after chemical attack: a) TCP, b) 1Z-TCP and c) 1Z-1M-TCP.

Fig. 7 shows the values of E and Hv obtained in the SPS samples. In both cases, a slight increase of E and Hv in doped samples with respect to undoped sample was observed. E values of doped samples were very similar while Hv values show a slight growing when dopant content increases. Considering that undoped sample shows very low intergranular porosity with respect to doped samples, the slight variations found in the E values can be attributed to this fact. In the case of Hv values, the slight increase observed could be caused by the grain size evolution, which decreases in the codoped samples. Its high density/low porosity, higher shrinkage and chemical bond strength also enhanced the hardness of these samples.

Fig. 8 shows the evolution of the modulus of elasticity and the Vickers microhardness as a function of the sintering temperature for samples obtained by SPS and conventional sintering. In this figure, values of E and Hv taken from the literature have been included and correspond to studies carried out on dense materials and thick films based on undoped TCP [14,40,41].

The materials obtained by SPS show a very significant increase in the values of Hv and E with respect to those obtained through different conventional sintering processes from different sources [14,40,41]. The improvement observed in both mechanical parameters is directly related to the high density and the limited grain growth of the grain size reached

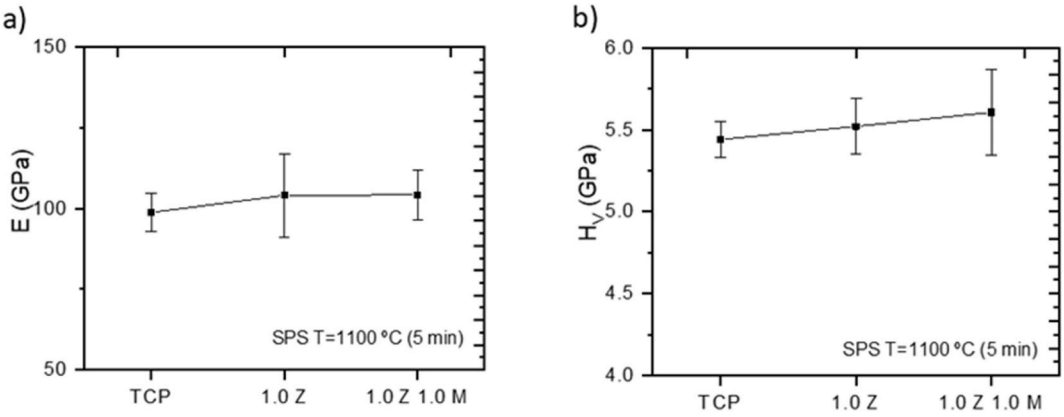

Fig. 7. a) Modulus of elasticity (E) and b) Vickers microhardness (Hv) of SPS samples.

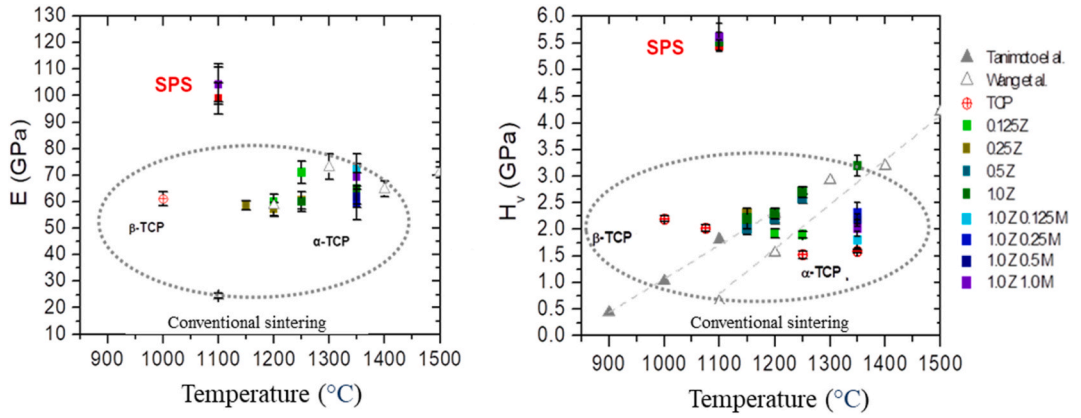

Fig. 8. Evolution of Modulus of elasticity (E) and Vickers microhardness (Hv) as a function of temperature of obtained SPS samples and conventional sintering samples taken from literature [14,40,41] and obtained by present authors.

in SPS samples. In this sense, it has been observed that the reduction of almost an order of magnitude in the average grain size of the samples 1Z-TCP sintered at 1100 °C by SPS (0.5–1.5 μm) with respect to those sintered through conventional sintering methods (10–25 μm), produces an increase of the order of 40% in the value of modulus of elasticity and almost 100% in the Vickers hardness values. These results are obviously a consequence of Zn^{2+} and Zn^{2+}/Mg^{2+} doping which are able to improve the thermal stability of TCP [13,15,28,30,42].

3.4. Biological behavior. Direct interaction cell-TCP dense sample

A comparative study of biological behavior of undoped-TCP, 1Z-TCP and 1Z-1M-TCP samples, specifically direct interaction cells-surface of biomaterials has been done. Tests were carried out through the immersion polished dense samples in a culture media (DMEM + 10% + bovine fetal serum + 1% v/v penicillin/glutamine), of MG-63 osteosarcoma human cells (osteoblastic type cells), previously incubated for 48 h.

Considering that there are many variables (micro and submicroroughness, macro and microporosity) that influence this type of test, all samples were previously polished to avoid topographical differences such as roughness. The polished samples presented similar values of surface roughness, Ra = 0.8 ± 0.1 μm and Rz = 5.0 ± 0.9 μm, being Ra the arithmetical average roughness of the surface and Rz the difference between the tallest "peak" and the deepest "valley" in the surface, the mean roughness depth. Porosity of samples was also very similar in the range of 0.5% ± 0.1. A qualitative analysis of cells adhesion, morphology and distribution on the polished surface of samples was performed using a Confocal Laser Scanning Microscopy after an incubation of 48 h. Fig. 9 shows the results obtained. The green color is obtained by staining the cytosol of living cells.

A high adhesion and cell propagation was achieved on samples surfaces. Cells present intimate contact and typical osteoblast morphology with an extended polygonal shape. Moreover, cells developed numerous cytoplasmic extensions that project off the main cell body, some of which have been pointed in Fig. 9. These extensions connect with the extensions of other neighboring osteocytes developing an osteocyte lacunar-canalicular networks and improving/speeding up osseointegration of implants [43].

The observation of the surface of the samples evidences that in the doped samples the cells reach a greater physical contact between them, improving adhesion and cellular morphology. It is relevant that zinc doped sample, 1Z-TCP, seems to show a slightly better behavior with respect to 1Z-1M-TCP since generated a dense and confluent layer that covers practically the entire surface of the material. This result allows us to deduce that Zn^{2+} significantly improves the biological interaction between cells and surface of biomaterial while the joint incorporation of Mg^{2+} and Zn^{2+} to TCP does not produce an improvement effect on this biological behavior. In fact, it is equal to or very slightly less.

The described SPS process allows opening a way to obtain implants with the desired microstructure, better mechanical-biological properties combination for custom orthopedic applications.

4. Conclusions

Spark Plasma Sintering (SPS) technique has allowed obtaining β-tricalcium phosphate at lower temperatures and much shorter treatment times and for the first time Zn-doped and ZnMg-codoped TCP materials with high density, very low porosity and low grain growth.

The codoped 1Z-1M-TCP materials obtained by CS and SPS processes presented a densification-sintering process at higher temperatures and greater contraction compared to undoped and zinc doped TCP materials.

Samples obtained by SPS showed a grain size of an order of magnitude smaller with respect to CS sintered samples and as a consequence

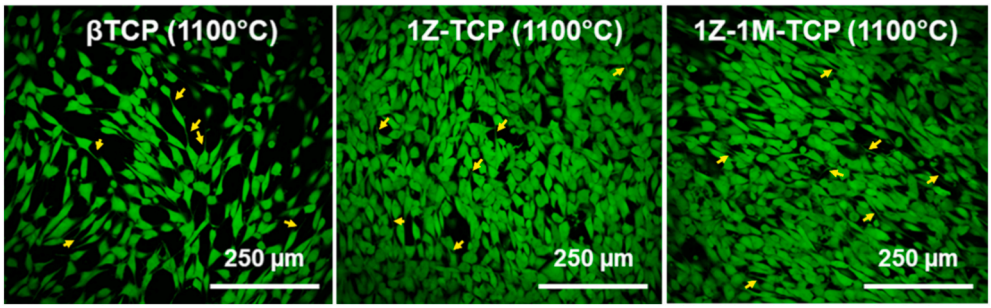

Fig. 9. Polished surface of dense SPS samples after 48 h of direct interaction with MG-63 cells observed by Confocal Laser Scanning Microscopy. a) undoped-TCP, b) 1Z-TCP and c) 1Z-1M-TCP.

an increase of the around 40% in the elastic modulus and close to 100% in Vickers hardness was obtained.

The incorporation of Zn^{2+} and Zn^{2+} plus Mg^{2+} in β-TCP materials produces a greater physical contact between cells and materials, improving adhesion and cellular morphology in tests of direct interaction between human cells (MG-63) and samples. Nevertheless, Zn^{2+} play a more relevant role than Mg^{2+} since incorporation on Mg^{2+} to Zn-doped sample does not produce an improvement effect on its biological behavior.

Finally, SPS process together with the Zn and Mg dopants have a synergistic effect that enhanced sinterability and densification of TCP and, as a consequence, improved the mechanical and biological properties of Zn, Zn–Mg TCP based materials.

Contributors

Maria Antonia Sainz* y Angel Caballero participated in the study design, analysis, and report development, interpretation of study findings and in writing the paper. Sara Serena participated in assessment of data quality, interpretation of study findings and in writing the paper. All authors participated in revision of the report and approved the final version. *Corresponding author: Tel: +34 91 735 58 40 Ext: 441,949 E-mail: masainz@icv.csic.es.

Declaration of competing interest

The authors declare that they have no known competing financial interests or personal relationships that could have appeared to influence the work reported in this paper.

Acknowledgments

This work is supported by the MICINN (Spain) with project CSIC 2017–60E028 and MCIU/AEI/FEDER (UE) with project RTI2018-095052-B-100. The authors wish thank Leticia Carbajal for her collaboration in obtaining the materials.

References

[1] P. Frayssinet, L. Trouillet, N. Rouquet, E. Azimus, A. Autefage, Osseointegration of macroporous calcium phosphate ceramics having a different chemical composition, Biomaterials 14 (1993) 423–429, https://doi.org/10.1016/0142-9612(93)90144-Q.

[2] J.-W. Choi, Y.-M. Kong, H.-E. Kim, Reinforcement of hydroxyapatite bioceramic by addition of Ni_3Al and Al_2O_3, J. Am. Ceram. Soc. 81 (7) (1998) 1743–1748, https://doi.org/10.1111/j.1151-2916.1998.tb02543.x.

[3] J.A. Juhasz, S.M. Best, Bioactive ceramics: processing, structures and properties, J. Mater. Sci. 47 (2012) 610–624, https://doi.org/10.1007/s10853-011-6063-x.

[4] E.R. Kreidler, F.A. Hummel, Phase equilibria in the system $Ca_3(PO_4)_2$-$Zn_3(PO_4)_2$, Inorg. Chem. 6 (1967) 524–528, https://doi.org/10.1021/ic50049a021.

[5] S. Serena, L. Carbajal, M.A. Sainz, A. Caballero, Thermodynamic assessment of the system CaO-P_2O_5: application of the ionic two-sublattice model to glass-forming melts, J. Am. Ceram. Soc. 94 (2011) 3094–3103, https://doi.org/10.1111/j.1551-2916.2011.04834.x.

[6] S. Kwon, Y. Jun, S. Hong, I. Lee, H. Kim, Calcium phosphate bioceramics with various porosities and dissolution rates, J. Am. Ceram. Soc. 85 (12) (2002) 3129–3131, https://doi.org/10.1111/j.1151-2916.2002.tb00599.x.

[7] S.J. Kalita, A. Bhardwaj, H. Bhatt, Nanocrystalline calcium phosphate ceramics in biomedical engineering, Mater. Sci. Eng. C 27 (2007) 441–449, https://doi.org/10.1016/j.msec.2006.05.018.

[8] M. Frasnelli, V.M. Sglavo, Flash sintering of tricalcium phosphate (TCP) bioceramics, J. Eur. Ceram. Soc. 38 (1) (2018) 279–285, https://doi.org/10.1016/j.jeurceramsoc.2017.08.004.

[9] F. Zhang, K. Lin, J. Changa, J. Lua, C. Ning, Spark plasma sintering of macroporous calcium phosphate scaffolds from nanocrystalline powders, J. Eur. Ceram. Soc. 28 (2008) 539–545, https://doi.org/10.1016/j.jeurceramsoc.2007.07.012.

[10] D. Kawagoe, K. Ioku, H. Fujimori, S. Goto, Transparent β-Tricalcium phosphate ceramics prepared by spark plasma sintering, J. Ceram. Soc. Jpn. 112 (8) (2004) 462–463, https://doi.org/10.2109/jcersj.112.462.

[11] A. Galotta, V.M. Sglavo, The cold sintering process: a review on processing features, densification mechanisms and perspectives, J. Eur. Ceram. Soc. 41 (16) (2021) 1–17, https://doi.org/10.1016/j.jeurceramsoc.2021.09.024.

[12] K. Rubenis, S. Zemjane, J. Vecstaudza, J. Bitenieks, J. Locs, Densification of amorphous calcium phosphate using principles of the cold sintering process, J. Eur. Ceram. Soc. 41 (2021) 912–919, https://doi.org/10.1016/j.jeurceramsoc.2020.08.074.

[13] L. Carbajal, A. Caballero, M.A. Sainz, Design and processing of ZnO doped tricalcium phosphate based materials: influence of β/α polymorph phase assemblage on microstructural evolution, J. Eur. Ceram. Soc. 32 (3) (2012) 569–577, https://doi.org/10.1016/j.jeurceramsoc.2011.09.025.

[14] L. Carbajal, S. Serena, A. Caballero, M.A. Saínz, R. Detsch, A.R. Boccaccini, Role of ZnO additions on the β/α phase relation in TCP based materials: phase stability, properties, dissolution and biological response, J. Eur. Ceram. Soc. 34 (5) (2014) 1375–1385, https://doi.org/10.1016/j.jeurceramsoc.2013.11.010.

[15] M. Frasnelli, V.M. Sglavo, Effect of Mg^{2+} doping on beta-alpha phase transition in tricalcium phosphate (TCP) bioceramics, Acta Biomater. 33 (2016) 283–289, https://doi.org/10.1016/j.actbio.2016.01.015.

[16] L. Prashanth, K.K. Kattapagari, R.T. Chitturi, V.R. Baddam, L.K. Prasad, A review on role of essential trace elements in health and disease, J NTR Univ Health Sci 4 (2015) 75–85. https://www.jdrntruhs.org/text.asp?2015/4/2/75/158577.

[17] M. Yamaguchi, Role of zinc in bone formation and bone resorption, J. Trace Elem. Exp. Med. 11 (1998) 119–135, https://doi.org/10.1002/(SICI)1520–670X(1998)11:2/3<119::AID-JTRA5>3.0.CO;2-3.

[18] Y-C. Yang, C.C. Chen, J-B. Wang, Y-C. Wang, F-H. Lin. Flame sprayed zinc doped hydroxyapatite coating with antibacterial and biocompatible properties, https://doi.org/10.1016/j.ceramint.2017.05.318.

[19] A. Bhattacharjee, A. Gupta, M. Verma, P.A. Murugan, P. Sengupta, S. Matheshwaran, Site-specific antibacterial efficacy and cyto/hemo-compatibility of zinc substituted hydroxyapatite, Ceram. Int. 45 (9) (2019) 12225–12233, https://doi.org/10.1016/j.ceramint.2019.03.132.

[20] E.S. Thian, T. Konishi, Y. Kawanobe, P.N. Lim, C. Choong, B. Ho, Zinc-substituted hydroxyapatite: a biomaterial with enhanced bioactivity and antibacterial properties, J. Mater. Sci. Mater. Med. 24 (2) (2013) 437–445, https://doi.org/10.1007/s10856-012-4817-x.

[21] T.N. Kim, Q.L. Feng, J.O. Kim, J. Wu, H. Wang, G.C. Chen, F.Z. Cui, Antimicrobial effects of metal ions (Ag^{+}, Cu^{2+}, Zn^{2+}) in hydroxyapatite, J. Mater. Sci. Mater. Med. 9 (3) (1998) 129–134, https://doi.org/10.1023/A:1008811501734.

[22] S. Yoshizawa, A. Brown, A. Barchowsky, C. Sfeir, Magnesium ion stimulation of bone marrow stromal cells enhances osteogenic activity, simulating the effect of magnesium alloy degradation, Acta Biomater. 10 (6) (2014) 2834–2842. https://doi:10.1016/j.actbio.2014.02.002.

[23] M. Diba, O.M. Goudouri, F. Tapia, A.R. Boccaccini, Magnesium-containing bioactive polycrystalline silicate-based ceramics and glass-ceramics for biomedical applications, Curr. Opin. Solid State Mater. Sci. 18 (3) (2014) 147–167, https://doi.org/10.1016/j.cossms.2014.02.004.

[24] Z. Wu, T. Tang, H. Guo, S. Tang, Y. Niu, J. Zhang, W. Zhang, R. Ma, J. Su, C. Liu, In Vitro degradability, bioactivity and cell responses to mesoporous magnesium silicate for the Induction of bone regeneration, Colloids Surf., B 120 (2014) 38–46. https://doi:10.1016/j.colsurfb.2014.04.010.

[25] A. Hartwig, Role of magnesium in genomic stability, Mutat. Res. 475 (1–2) (2001 Apr 18) 113–121. PMID: 11295157, https://doi:10.1016/s0027-5107(01)00074-4.

[26] L. Carbajal, M.A. Sainz, S. Serena, A.C. Caballero, A. Caballero, Solid-state compatibility in two regions of the system ZnO-CaO-P_2O_5, J. Am. Ceram. Soc. 94 (2011) 2213–2219, https://doi.org/10.1111/j.1551-2916.2010.04355.x.

[27] R.G. Carrodeguas, A.H. De Aza, X. Turrillas, P. Pena, S. De Aza, New approach to the β→α polymorphic transformation in magnesium-substituted tricalcium phosphate and its practical implications, J. Am. Ceram. Soc. 91 (2008) 1281–1286, https://doi.org/10.1111/j.1551-2916.2008.02294.x.

[28] L. Carbajal, S. Serena, M.A. Sainz, A. Caballero, Phase and melting relationships of β, α and α′-$Ca_3(PO_4)_2$ polymorphs in the $Ca_3(PO_4)_2$ -$Zn_3(PO_4)_2$ system, J. Eur. Ceram. Soc. 37 (5) (2017) 2277–2283, https://doi.org/10.1016/j.jeurceramsoc.2016.12.022.

[29] M. Tokita, Progress of spark plasma sintering (SPS) method, systems, ceramics applications and industrialization, Ceramics 4 (2021) 160–198, https://doi.org/10.3390/ceramics4020014.

[30] S. Kannan, F. Goetz-Neunhoeffer, J. Neubauer, S. Pina, P.M.C. Torres, J.M. F. Ferreira, Synthesis and structural characterization of strontium- and magnesium-co-substituted β-tricalcium phosphate, Acta Biomater. 6 (2010) 571–576, https://doi.org/10.1016/j.actbio.2009.08.009.

[31] K. Kawabata, T. Yamamoto, A. Kitada, Substitution mechanism of Zn ions in β-tricalcium phosphate, Phys. B Condens. Matter 406 (2011) 890–894, https://doi.org/10.1016/j.physb.2010.12.022.

[32] G. Renaudin, S. Gomes, J.-M. Nedelec, First-row transition metal doping in calcium phosphate bioceramics: a detailed crystallographic study, Materials 10 (1) (2017) 92, https://doi.org/10.3390/ma10010092.

[33] M. Ikeuchi, A. Ito, Y. Dohi, H. Ohgushi, H. Shimaoka, K. Yonemasu, T. Tateishi, Osteogenic differentiation of cultured rat and human bone marrow cells on the surface of zinc-releasing calcium phosphate ceramics, Biomed. Mater. Res. 67 (2003) 1115–1122, https://doi.org/10.1002/jbm.a.10041.

[34] T. Lu, X. Yuan, L. Zhang, F. He, X. Wang, Y. Zhang, J. Ye, High throughput synthesis and screening of zinc-doped biphasic calcium phosphate for bone regeneration, Appl. Mater. Today 25 (2021), https://doi.org/10.1016/j.apmt.2021.101225 article 101225.

[35] W. Oliver, G. Pharr, An improved technique for determining hardness and elastic modulus using load and displacement sensing indentation experiments, J. Mater. Res. 7 (6) (1992) 1564–1580, https://doi.org/10.1557/JMR.1992.1564.

[36] K.E. Amin, Toughness, hardness and wear, engineered materials handbook, in: Ceramics and Glasses, 4, ASM International, New York, 1991, pp. 599–609, 0-87170-282-7.

[37] I.N. Sneddon, The relation between load and penetration in the axisymmetric problem for a punch of arbitrary profile, Int. J. Eng. Sci. 3 (1965) 45–57, https://doi.org/10.1016/0020-7225(65)90019-4.
[38] S. Yamadi, S. Kobayashi, Effects of strain rate on the mechanical properties of tricalcium phosphate/poly (L-Lactide) composites, J. Mater. Sci. Mater. Med. 20 (1) (2009) 67–74, https://doi.org/10.1007/s10856-008-3553-8.
[39] A.C.S. Dantas, P. Greil, F.A. Müller, Effect of CO_3^{2-} incorporation on the mechanical properties of wet chemically synthesized B-tricalcium phosphate (TCP) ceramics, J. Am. Ceram. Soc. 91 (3) (2008) 1030–1033. https://doi:10.1111/j.1551-2916.2007.02208.x.
[40] Y. Tanimoto, N. Nishiyama, Preparation and physical properties of tricalcium phosphate laminates for bone-tissue engineering, J. Biomed. Mater. Res. A. 85 (2) (2008) 427–433, https://doi.org/10.1002/jbm.a.31569.
[41] C.X. Wang, X. Zhou, M. Wang, Influence of sintering temperatures on hardness and Young's modulus of tricalcium phosphate bioceramic by nanoindentation technique, Mater. Char. 52 (4–5) (2004) 301–307, https://doi.org/10.1016/j.matchar.2004.06.007.
[42] P. Nandha Kumar, J.M. da Fonte Ferreira, S. Kannan, Formation Mechanisms in β-$Ca_3(PO_4)_2$-ZnO composites: structural repercussions of composition and heat treatments, Inorg. Chem. 56 (3) (2017) 1289–1299, https://doi.org/10.1021/acs.inorgchem.6b02445.
[43] X. He, M. Yamada, J. Watanabe, J, I. Mizoguchi, I, H. Egusa, Titanium nanotopography induces osteocyte lacunar-canalicular networks to strengthen osseointegration, Acta Biomater. 151 (2022) 613–627, https://doi.org/10.1016/j.actbio.2022.08.023.